Collisions of low-energy electrons with CO 2

Chuo-Han Lee, Carl Winstead, and Vincent McKoy

Citation: The Journal of Chemical Physics **111**, 5056 (1999); doi: 10.1063/1.479761
View online: http://dx.doi.org/10.1063/1.479761
View Table of Contents: http://scitation.aip.org/content/aip/journal/jcp/111/11?ver=pdfcov
Published by the AIP Publishing

Collisions of low-energy electrons with CO_2

Chuo-Han Lee, Carl Winstead, and Vincent McKoy[a)]
A. A. Noyes Laboratory of Chemical Physics, California Institute of Technology, Pasadena, California 91125

(Received 8 December 1998; accepted 8 June 1999)

We report cross sections for collisions of low-energy electrons with carbon dioxide obtained by the Schwinger multichannel variational method. Elastic cross sections are obtained in the static-exchange-plus-polarization approximation. We pay particular attention to the position of the $^2\Pi_u$ resonance and to the strong enhancement in the integral cross section near zero energy, both prominent features whose accurate treatment requires an accounting for polarization effects. To include such effects in the resonant symmetry, we use an objective and physically motivated criterion to construct a set of configurations that accurately accounts for polarization while avoiding overcorrelation. In addition, we study the origin of the nonisotropic behavior of the elastic differential cross section at very low energies and conclude that it is caused by significant contributions from vibrationally excited CO_2. Cross sections from threshold to 50 eV for excitation of the $^3\Sigma_u^+$, $^1\Delta_u$, $^3\Delta_u$, $^3\Sigma_u^-$, and $^1\Sigma_u^-$ states that arise from the $(1\pi_g \rightarrow 2\pi_u)$ transition are presented for the first time. © *1999 American Institute of Physics.* [S0021-9606(99)01633-5]

I. INTRODUCTION

Collisions of low-energy electrons with carbon dioxide, both elastic and inelastic, play an important role in planetary atmospheres, gas lasers, and low-temperature plasmas.[1] Since the first measurements of the total cross sections for electron–CO_2 collisions were reported in 1927,[2,3] several studies of low-energy total and elastic[4–28] and vibrationally inelastic[29–49] scattering have been published. To our knowledge, there have been no measurements of cross sections for electronic excitation of CO_2 by low-energy electrons, and only one calculation, for intermediate energies.[50]

We have formulated and exploited the Schwinger multichannel (SMC) variational method[51–53] to obtain the cross sections for collisions of low-energy electrons with several molecules. For example, we have reported elastic cross sections for CF_4,[54] PH_3,[55] and AsH_3,[55] and electronically inelastic cross sections for H_2O,[56] H_2CO,[57] CO,[58] CH_4,[59] and SiH_4.[60] Here, we report elastic and inelastic cross sections for electron scattering by CO_2. In our elastic scattering studies, we pay particular attention to two features of the elastic integral cross section whose accurate description requires inclusion of polarization effects.[16,21,23] The first is the well-known $^2\Pi_u$ resonance near 3.8 eV, which static-exchange calculations generally place about 2 eV too high. The dominant partial wave of this resonance has not been conclusively identified.[16,18,21,24,38,61,62] The second is the strong enhancement in the cross section near zero energy. This enhancement has generally been ascribed to the presence of an *s*-wave virtual state.[63–66] This explanation implies that the scattering should be isotropic at low energies. However, the measured differential cross sections[12] show significant forward scattering. To date, there has been no satisfactory explanation of this inconsistency. In the present study, we show that this discrepancy between theory and experiment can be resolved by recognizing that the measured values contain contributions from vibrationally excited states, whose elastic cross sections are forward peaked.

We also report integral and differential cross sections for electronic excitation of CO_2. Results of both a three-channel, two-state calculation ($X\,^1\Sigma_g^+, ^3\Sigma_u^+$) and a nine-channel, six-state calculation ($X\,^1\Sigma_g^+, ^3\Sigma_u^+, ^1\Delta_u, ^3\Delta_u, ^3\Sigma_u^-, ^1\Sigma_u^-$) are presented. All of these excited states arise from the $(1\pi_g \rightarrow 2\pi_u)$ transition and are valence in nature. Calculations in which a large number of open channels is included are quite demanding computationally, and the high-performance computing provided by massively parallel computers facilitates such applications.

In Sec. II our theoretical approach is briefly summarized. Section III describes the computational procedure, and Sec. IV contains our results and discussion. Concluding remarks are given in Sec. V.

II. THEORETICAL METHOD

The SMC method has been fully described elsewhere,[51–53] and here we simply present some of its key features. The variationally stable expression for the scattering amplitude is

$$f(\mathbf{k}_m,\mathbf{k}_n) = -\frac{1}{2\pi}\sum_{ij}\langle S_m(\mathbf{k}_m)|V|\chi_i\rangle \times (A^{-1})_{ij}\langle\chi_j|V|S_n(\mathbf{k}_n)\rangle, \tag{1}$$

where A^{-1} is the inverse of the matrix representative of the operator

$$A^{(+)} = \tfrac{1}{2}(PV+VP) - VG_P^{(+)}V - \frac{1}{N+1}\left[\hat{H} - \frac{N+1}{2}(\hat{H}P+P\hat{H})\right], \tag{2}$$

a)Electronic mail: mckoy@cco.caltech.edu

with $\hat{H}$ the total energy minus the Hamiltonian of the system, N the total number of electrons in the target, P a projection operator onto the open electronic channels of the target, and $G_P^{(+)}$ the projected free-particle Green's function. The functions S_m and S_n in Eq. (1) are the interaction-free solutions, i.e.,

$$S_m(\mathbf{k}_m) = \Phi_m(\mathbf{r}_1,\ldots,\mathbf{r}_N)\exp(i\mathbf{k}_m\cdot\mathbf{r}_{N+1}), \tag{3}$$

Φ_m being an eigenstate of the target. The $\chi_i(\mathbf{r}_1,\mathbf{r}_2,\ldots,\mathbf{r}_{N+1})$ are basis functions—$(N+1)$-electron configuration state functions—in which the total trial scattering wave function is expanded. We have previously shown that, as in the original Schwinger method, the SMC trial wave function need not satisfy scattering boundary conditions; thus, square-integrable functions such as Cartesian Gaussians may be used to construct the χ_i. In fact, if the orbitals in χ_i are expanded in Cartesian Gaussian functions, all integrals needed in the construction of the matrix elements in Eq. (1) can be evaluated analytically, except those arising from the $VG_P^{(+)}V$ term. These terms are evaluated using a quadrature scheme that is particularly well suited for implementation on distributed-memory parallel computers.[67]

As mentioned in Sec. I, an accurate description of the scattering at low energies requires the inclusion of polarization effects. A detailed description of our treatment of the polarization effects is presented elsewhere.[68] Here we only outline the important features. For the resonant symmetry, overcorrelation tends to occur if all virtual excitations of the target are included to describe polarization. A more effective approach is to restrict the closed-channel configurations to those contributing the most to polarization. Schneider and Collins[69] have noted that the target response in resonant symmetry can be mostly accounted for by ''radial correlation,'' or symmetry-preserving excitations. In a linear molecule such as CO_2, this corresponds to the $\sigma_g\rightarrow\sigma_g$, $\sigma_u\rightarrow\sigma_u$, $\pi_g\rightarrow\pi_g$, and $\pi_u\rightarrow\pi_u$ excitations. However, employing all configurations of the form $(\rho\gamma\rightarrow q\gamma)n\pi$, where $\rho\gamma$ is an occupied orbital, $q\gamma$ a virtual orbital of the same symmetry, and $n\pi$ a π virtual orbital, results in overcorrelation of the target. This problem is solved by constructing a valencelike virtual orbital $\tilde{\pi}$ and including only configurations of the form $(\rho\gamma\rightarrow q\gamma)\tilde{\pi}$. $\tilde{\pi}$ is constructed by using a cation Fock operator to obtain the virtual orbitals. For the study of the $^2\Pi_u$ symmetry of CO_2, we use a $+4$ Fock operator to preserve the equivalence of the two π_g orbitals.

For the nonresonant $^2\Sigma_g$ symmetry, the underlying physics is different,[68,69] and all dipole-allowed excitations are needed to represent this type of polarization. Unfortunately, such a description leads to many thousands of configurations for even modest-sized basis sets. To reduce the size of the calculation, a small set of ''polarizing'' orbitals is generated[68] such that only excitations into these orbitals are necessary to describe polarization. For a component χ_μ of the dipole operator and occupied orbital ϕ_i, the polarizing orbital is defined as

$$\phi_{i,\mu} = N_{i,\mu}\sum_j \phi_j\langle\phi_j|\chi_\mu|\phi_i\rangle, \tag{4}$$

where the sum runs over virtual orbitals and $N_{i,\mu}$ is a normalization factor. In order to maintain an orthogonal set of virtual orbitals, we Schmidt orthogonalize the polarizing orbitals constructed for different target orbitals among themselves, then Schmidt orthogonalize the remaining virtual orbitals to the polarizing orbitals.

TABLE I. Diffuse and polarization functions used in the present calculation. These functions are added to the $(9s5p)/(5s3p)$ basis of Dunning.[a]

Atom	Function type	Basis I	Basis II	Basis III
Carbon	s	0.061 32	0.061 32	0.05
			0.01	0.02
				0.01
				0.004
	p	0.045	0.045	0.05
			0.015	0.02
				0.007
	d	1.5	1.5	1.097
		0.75	0.75	0.318
		0.3	0.3	0.09
			0.05	
Oxygen	s	0.113 84	0.113 84	0.065
				0.026
				0.013
				0.0052
	p	0.08	0.08	0.08
				0.026
				0.0091
	d	1.7	1.7	1.426
		0.85	0.85	0.4134
		0.34	0.34	0.117
			0.12	

[a]Reference 70

III. CALCULATIONS

All calculations are carried out at the experimental C–O internuclear distance of 2.9144 a.u. In the calculation of elastic cross sections, we include polarization effects only in the $^2\Sigma_g$ and $^2\Pi_u$ symmetries; in the other symmetries—$^2\Sigma_u$, $^2\Pi_g$, $^2\Delta_g$, and $^2\Delta_u$—including polarization results in minimal changes in the cross sections, so the static-exchange results are used. Several Cartesian Gaussian basis sets are employed in our work to ensure convergence of the cross sections. These Gaussian basis sets consist of a set of valence-type functions augmented by a set of diffuse and polarization functions. The valence-type set is Dunning's $(9s5p)/[5s3p]$ for both carbon and oxygen,[70] and the latter set is given in Table I. Because several calculations are performed, each with a different purpose, three sets of diffuse and polarization functions are used. Note that we use the full set of six Cartesian d Gaussians for each exponent. The $^2\Pi_u$ calculation uses basis I, which gives a self-consistent field (SCF) energy of $-187.698\,29$ a.u. The static-exchange calculation uses basis II, which gives a SCF energy of $-187.698\,76$ a.u. Basis II contains more diffuse and polarization functions to enable a better description of the higher partial waves, whose contributions become important at

TABLE II. Comparison of calculated vertical excitation energies with other theoretical and experimental results.

	Vertical threshold (eV)				
		Previous calculation		Experiment	
State	This work	Ref. 74	Ref. 75	Ref. 76	Ref. 77
$^1\Delta_u$	9.95	8.38	9.43	8.41	8.4–8.6
$^3\Delta_u$	9.13	7.83	9.02		8.1
$^3\Sigma_u^+$	8.53	7.35	8.65	4.89	
$^3\Sigma_u^-$	9.73	8.24	9.42		8.3
$^1\Sigma_u^-$	9.73	8.27	9.42	6.53	8.3

higher energies. The $^2\Sigma_g$ calculation used basis III, which has extra *s* and *p* functions to ensure an accurate description of the low-energy region. The SCF energy for this basis is $-187.696\,18$ a.u. The near-Hartree–Fock limit for CO_2 is $-187.699\,58$ a.u.[71]

The three- and nine-channel calculations of the electron-impact excitation cross sections are performed with basis I. For the $(1\pi_g \rightarrow 2\pi_u)$ valence excited states of interest here, we use the improved virtual orbital (IVO) approximation,[72,73] in which the excited orbital $(2\pi_u)$ is determined as an eigenfunction of a Hamiltonian containing the potential produced by the unrelaxed $[1\sigma_g^2 1\sigma_u^2 2\sigma_g^2 3\sigma_g^2 2\sigma_u^2 4\sigma_g^2 3\sigma_u^2 1\pi_u^4 1\pi_g^3]$ core built from the ground state orbitals. The vertical excitation energies are compared to other calculated[74,75] and measured[76,77] results in Table II. Configurations associated with channels other than the ground and $(1\pi_g \rightarrow 2\pi_u)$ states, whether open or closed, are excluded in the three- and nine-channel calculations. The representation of polarization effects is thus less complete than in the calculation of the elastic cross section.

All the states arising from the $(1\pi_g \rightarrow 2\pi_u)$ transition are formed by taking appropriate linear combinations of excited configurations, since the degeneracy of the π orbitals precludes a single-configuration description. In constructing $^3\Sigma_u^+$, two such configurations, or channels, are necessary, meaning that a calculation coupling the $X\,^1\Sigma_g^+$ and $^3\Sigma_u^+$ states requires three channels. Similarly, nine different channels are necessary to form the $X\,^1\Sigma_g^+$, $^3\Sigma_u^+$, $^3\Sigma_u^-$, $^1\Sigma_u^-$, $^1\Delta_u$, and $^3\Delta_u$ states. The $^1\Sigma_u^+$ state that nominally arises from the $(1\pi_g \rightarrow 2\pi_u)$ transition is of mixed Rydberg-valence character and is omitted in the present study because its accurate description requires going beyond the IVO model.

Only σ, π, and δ molecular orbitals can be formed from the nuclei-centered *s*, *p*, and *d* Gaussians included in our basis sets. Because the ground state symmetry is $^1\Sigma_g^+$ and the overall electronic symmetry is conserved, our calculations will include components of the total electronic wave function only up through $^2\Delta_{g,u}$. This is not expected to affect much the quality of the elastic results or, in general, that of the inelastic results, because the large angular momentum barrier in the entrance channel experienced by ϕ (leading partial wave $l=3$) and higher-*m* orbitals will preclude $^2\Phi$ and higher-Λ components from contributing strongly to low-energy scattering. A possible exception in the inelastic case is resonantly enhanced scattering via the $(1\pi_u)^3(2\pi_g)^2\,^2\Phi_u$ configuration. Our expectation is that any such resonant features would be weak, but it should be borne in mind that they are excluded from the outset in our calculations.

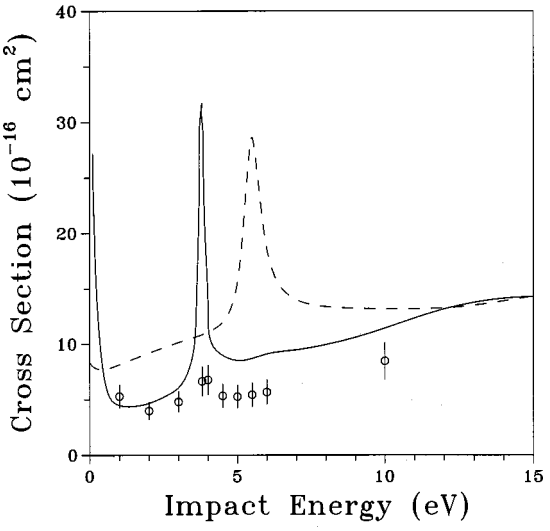

FIG. 1. Elastic scattering cross section for CO_2. Solid line—static-exchange-plus-polarization results; dashed line—static-exchange results; circles—measured vibrationally elastic cross section of Ref. 28.

IV. RESULTS AND DISCUSSION

A. Single-channel calculation

Figure 1 shows both our static-exchange (SE) and static-exchange-plus-polarization (SEP) elastic integral cross sections, along with measured values of Ref. 28. Clearly, our SE results do not place the $^2\Pi_u$ resonance at the correct position, nor do they reproduce the enhancement near zero energy. Similar SE results were reported by Morrison *et al.*,[16] Lucchese and McKoy,[21] and Gianturco and Stoecklin.[23]

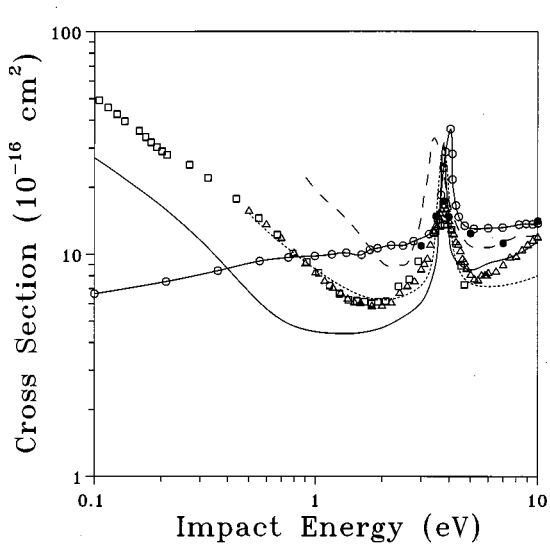

FIG. 2. Elastic electron scattering cross sections for CO_2. Solid line—present SEP results; long dashed line—model-potential calculation of Ref. 18; short dashed line—SEP calculation of Ref. 16; solid line with open circles—SEP calculation of Ref. 23; closed circles—measured elastic cross section of Ref. 5; open squares—measured total cross section of Ref. 8; open triangles—measured elastic cross section of Ref. 12.

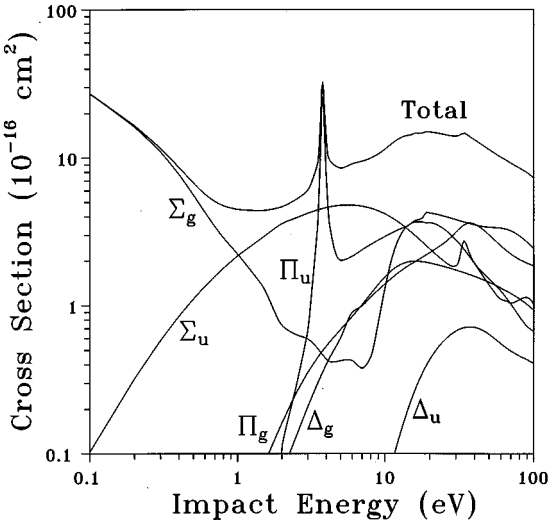

FIG. 3. Symmetry components of the electronically elastic scattering cross section for CO_2.

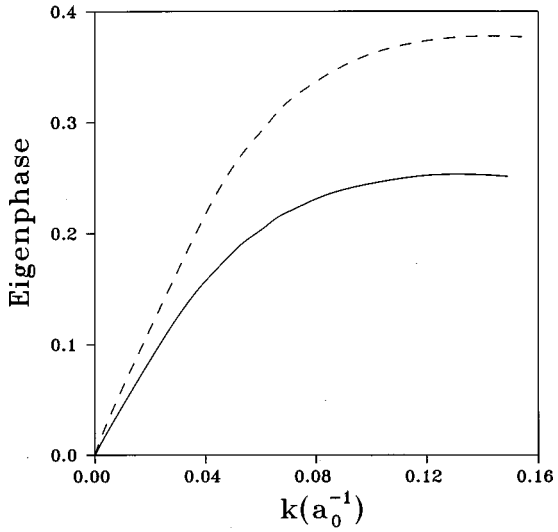

FIG. 5. Calculated *s*-wave eigenphases in $^2\Sigma_g$ symmetry. Solid line—present result; dashed line—calculation of Ref. 63.

Figure 2 shows an expanded view of our SEP elastic integral cross section and compares it with other elastic and total integral cross sections, both measured and calculated. Our results, along with those of Morrison *et al.*, who explicitly included a polarization potential, and those of Lynch *et al.*,[18] who implicitly included polarization effects in their continuum multiple-scattering model (CMSM),[78] demonstrate the importance of polarization in the region of the shape resonance and at very low energies. On the other hand, Gianturco and Stoecklin,[23] who described polarization using a density functional approach, placed the $^2\Pi_u$ resonance near the correct position but failed to describe correctly the behavior of the cross section near zero energy. The magnitude of our cross section at the peak of the resonance at 3.8 eV is too high for two reasons: First, we have neglected nuclear motion, which would broaden the resonance and reduce its peak value accordingly; second, we do not use a correlated target. Meyer *et al.*[79] and Ghose *et al.*[80] have shown that a correlated target is required to represent polarization effects fully.

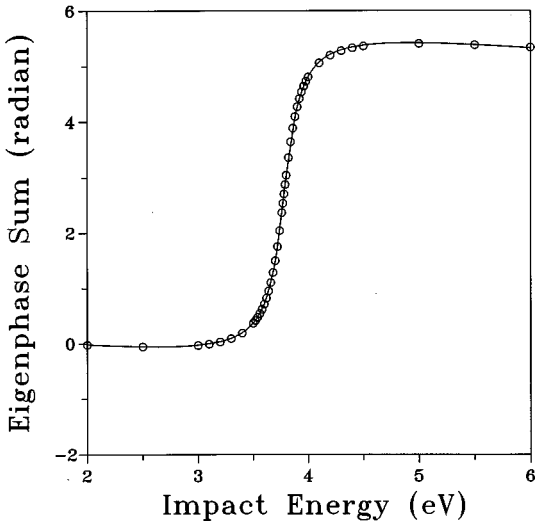

FIG. 4. Eigenphase sum in $^2\Pi_u$ symmetry near the resonance energy. The circles are the calculated points; the line is a fit to $\Delta(E) = -0.209 - 0.177E + 2\tan^{-1}[0.116/(3.780\text{-}E)]$. (The factor of 2 in the arctangent term arises from the twofold degeneracy of the resonance.)

Figure 3 shows the symmetry components of our calculated elastic integral cross section. At higher energies, we find two resonances. The first occurs in $^2\Sigma_g$ symmetry and leads to a rapid rise in the cross section between 10 and 15 eV, with a maximum at about 17 eV. Similar behavior is seen in the calculations of Lynch *et al.*[18] and of Gianturco and Stoecklin.[23] Tronc *et al.*,[37] in their study of vibrational excitation, observed a peak at 10.8 eV which they interpreted as the $^2\Sigma_g$ shape resonance predicted by Lynch *et al.*[18] There is obviously a large difference between the energies of the maximum in the calculated $^2\Sigma_g$ fixed-nuclei elastic cross section and of that seen in the vibrational excitation cross section of Tronc *et al.*[37] However, a fit of our calculated $^2\Sigma_g$ eigenphase sum to a Breit–Wigner form plus a low-order polynomial for the background yields a resonance position of 13.4 eV and a width of 8.2 eV. These values are similar to those obtained by Gianturco and Lucchese.[24] The large difference between the resonance energy and the location of the maximum in the cross section is due to the significant background phase shift, which is close to $3\pi/4$ near the resonance energy, leading to a highly asymmetric profile with a minimum below and a maximum above the resonance position (see Fig. 3). A resonance position of 13.4 eV makes it much more likely that this feature is indeed responsible for the resonant enhancement seen in the measured vibrational excitation cross sections.[37] A SCF calculation using a minimal basis set, whose virtual orbital energies correlate roughly with resonance positions, places a σ_g orbital at 12.9 eV.

The second high-energy resonance is a broad $^2\Sigma_u$ resonance around 34 eV, which again was observed at about the same energy in the calculations of Lynch *et al.*[18] The vibrational excitation cross section of Tronc[37] showed this resonance at 30 eV. The minimal-basis virtual σ_u orbital lies at 34 eV.

TABLE III. Scattering length of the *s*-wave virtual state.

Author	Scattering length (a_0)	Method
Present	−4.51	SMC calculation in the static-exchange-plus-polarization approximation
Morrison[a]	−6.17	Coupled-channel calculation with model static-exchange-plus-polarizationpotential
Singh[b]	−7.2	Derived from momentum transfer cross sections
Fabrikant[c]	−6.8 to −7.2	Calculation using effective-range theory and the Born approximation
Estrada and Domcke[d]	−7.82	Described the virtual state using a parametrizedmodel based on the projection-operator formalism of Feshbach with an optical potential
Morgan[e]	−4.95	*R*-matrix calculation

[a]Reference 63.
[b]Reference 81.
[c]Reference 82.
[d]Reference 65.
[e]Reference 66.

At lower energy, the well-known $^2\Pi_u$ resonance is prominent (Figs. 2 and 3). Our SEP calculation correctly locates the resonance position. A fit of the $^2\Pi_u$ eigenphase sum to the Breit–Wigner form plus a low-order polynomial representing the background yields 3.78 eV for the resonance position E_r and 0.23 eV for the width Γ (Fig. 4). As in most recent studies, we find that the *f*-wave dominates the resonance.

Below 10 eV, the $^2\Sigma_g$ component of our cross section decreases to a minimum (the small oscillations are numerical artifacts), then, near zero energy, shows the sharp rise seen experimentally. Morrison[63] attributed this enhancement to an *s*-wave virtual state. This hypothesis has been confirmed by a number of studies.[64–66] The scattering length of the virtual state can be calculated from the *s*-wave eigenphase. Figure 5 compares our *s*-wave eigenphase with that of Morrison, and Table III compares our calculated scattering length with other results.[63,65,66,81,82]

Although the *s*-wave virtual state can account for the observed enhancement of the integral cross section near zero energy, the measured differential cross sections (DCSs) exhibit strong forward peaking that cannot be explained by this mechanism, suggesting that we have neglected some other mechanism(s) that can produce forward scattering at low energies. Ordinary dipole scattering can be ruled out because CO_2 does not have a permanent dipole. Quadrupole scattering can also be ruled out because it leads to isotropic cross sections.[83,84] Another possible mechanism, scattering due to the instantaneous dipole moment resulting from zero-point motion, also cannot explain this DCS feature; although a quantitative description of this effect is not possible in a fixed-nuclei approximation, since the interaction time is comparable to the vibrational period at low collision energies, it can readily be demonstrated that the effect is too small to explain the observed forward peaking.

Another possible explanation is significant population of vibrationally excited states that on average have a bent geometry and thus a dipole moment that can lead to forward scattering. Hayashi and Nakamura[85] pointed out that CO_2 cross sections appear to depend on temperature. They proposed that the ground and vibrationally excited levels have different cross sections, with the temperature dependence of the observed cross section merely reflecting the change in relative population. Indeed, a significant portion of CO_2 exists in vibrationally excited states at temperatures common in measurements. The percentage of CO_2 molecules in the (01^10) state, i.e., one quantum in the bending mode, has been estimated to be 8.4% at 335 K and 21.9% at 520 K.[86,87] The (01^10) state should possess a dipole moment and thus a different elastic DCS than the ground state. The measured DCS would represent the weighted average of the DCSs of the ground state, the (01^10) state, and other vibrationally excited states. Our hypothesis is that the forward scattering observed in the measured DCSs arises from these vibrationally excited states. To test this hypothesis, we have cal-

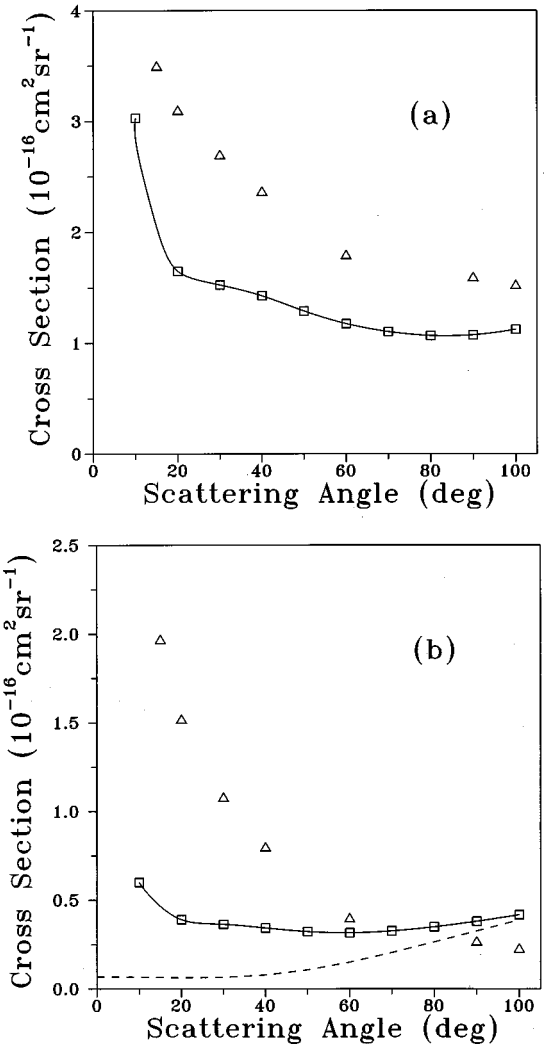

FIG. 6. Differential cross sections at (a) 0.155 eV and (b) 1.05 eV. Solid line with squares—present result; triangles—measurement of Ref. 12. The dashed line in (b) shows the present result without correction for vibrational excitation; see the text for discussion.

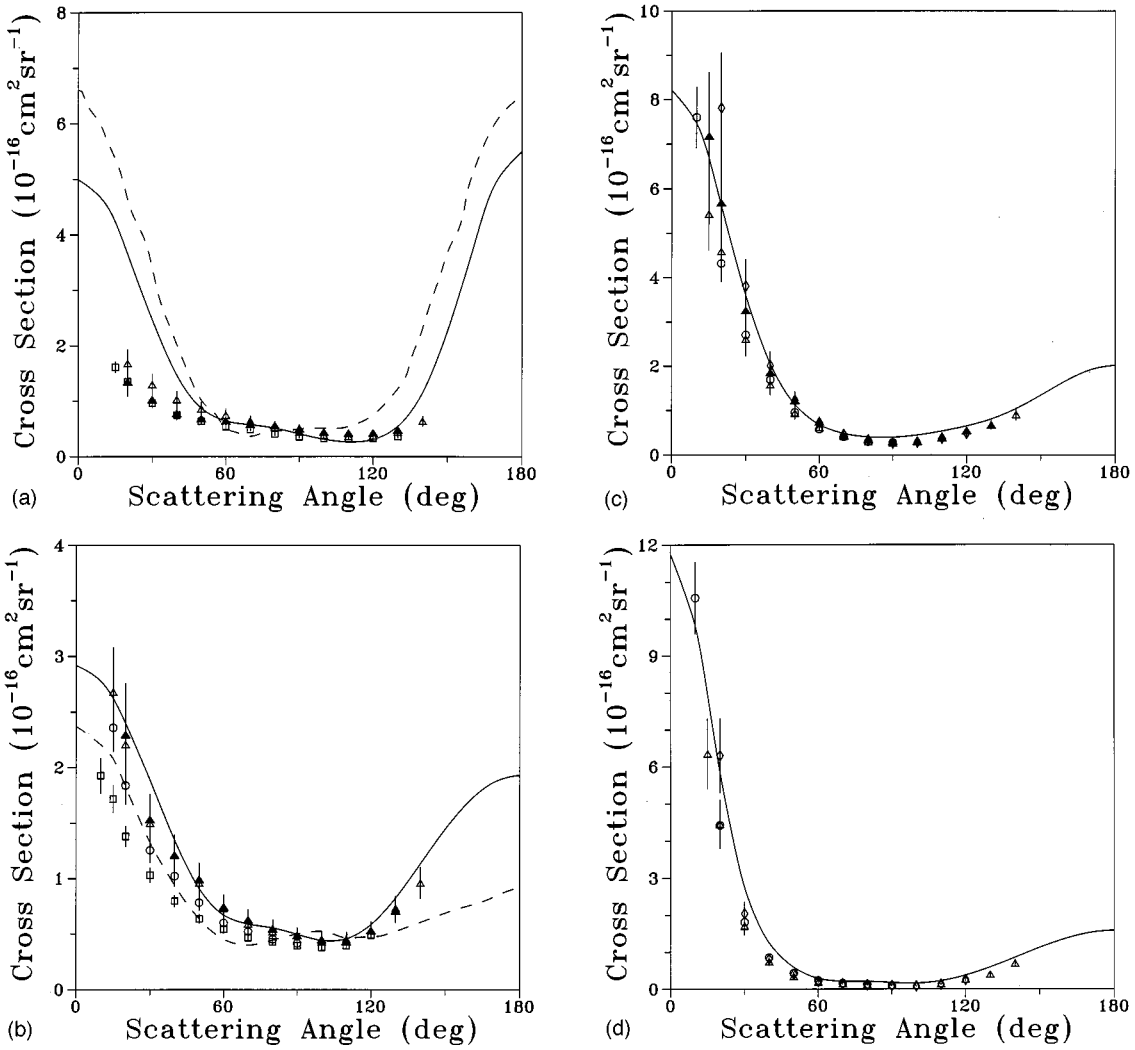

FIG. 7. Differential cross sections for elastic electron scattering by CO_2 at energies of (a) 4 eV, (b) 10 eV, (c) 20 eV, and (d) 50 eV. Solid line—present result; dashed line—calculation of Ref. 16; open triangle—measurement of Ref. 7; closed triangle—measurement of Ref. 27; open square—measurement of Ref. 28 (ANU); open circle—measurement of Ref. 28 (Flinders); open diamond—measurement of Ref. 14.

culated elastic cross sections for the three lowest vibrationally excited states of CO_2, namely (01^10), (02^00), and (02^20), while including a correction to account for the dipolar scattering. Since we are employing the fixed-nuclei approximation, and since, as noted above, the collision energy is too low for that approximation to be fully justified, we do not attempt a detailed average over nuclear positions; rather, a single bent geometry is used to represent each vibrationally excited state. Specifically, the calculations are performed at the ground state equilibrium C–O bond length and the respective rms O–C–O bond angles.[88] The population-weighted average of the DCSs for these vibrationally excited states and the ground state is then computed. Our results are not expected to be quantitative because of the limitations just mentioned, including the breakdown of the adiabatic approximation. Figure 6 shows our calculated DCSs at 0.155 and 1.05 eV, along with the measured results of Kochem *et al.*[12] We assume the population distribution at 520 K, the temperature inside the gas tube in the measurements of Kochem *et al.* At this temperature, the population of the lowest four states of CO_2 is 69.4% (0,0,0), 21.9% $(0,1^1,0)$, 2.0% $(0,2^0,0)$, and 3.5% $(0,2^2,0)$. These four states account for 96.8% of the population.[89]

At 0.155 eV, our DCS exhibits significant forward peaking and good qualitative agreement with the measured result. These results indicate that the forward-scattering enhancement observed in the elastic DCS of CO_2 is due to contributions from vibrationally excited states. At 1.05 eV, the agreement is not as good; our DCS shows only slight forward peaking. However, our DCS without the correction for vibrationally excited states, shown as a dashed line in Fig. 6(b), is in fact *backward* peaked, and the correction to the forward-scattering cross section is of the same order of magnitude as the observed forward peaking. Fully testing this hypothesis will require going beyond the adiabatic approximation.

Figure 7 shows our calculated elastic DCSs along with measurements of Register *et al.*,[7] Kanik *et al.*,[14] Tanaka *et al.*,[27] Gibson *et al.*,[28] and calculated values of Morrison *et al.*,[16] where available. At 4 and 10 eV, our calculated DCSs show a single minimum at about 100°, as do the measured values. At higher energies, our results agree well with

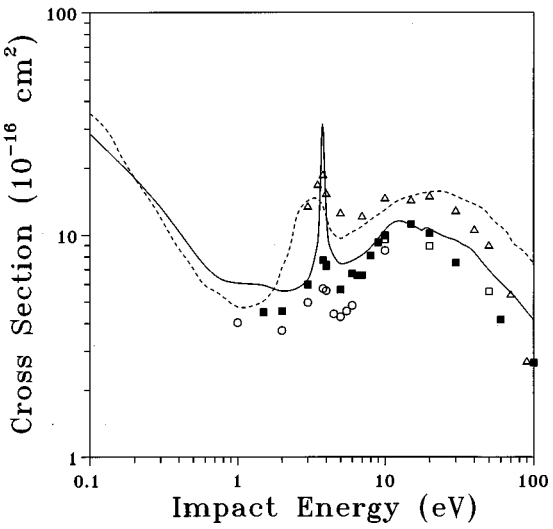

FIG. 8. Momentum-transfer cross section for $e^- - CO_2$ collisions. Experimentally derived values are from Refs. 4 (dashed line), 5 (open triangle), 7 (open square), 27 (closed square), and 28 (open circle); the solid line is the present calculation.

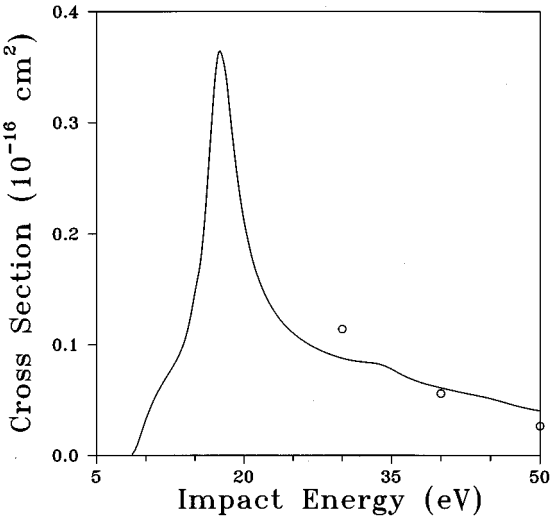

FIG. 9. Three-channel calculation of the $X\,^1\Sigma_g^+ \rightarrow {}^3\Sigma_u^+$ integral cross section. The circles are the DW results of Ref. 50.

the measurements in both magnitude and angular dependence.

The momentum-transfer cross section (MTCS) is shown in Fig. 8 along with the experimentally derived values of Lowke *et al.*,[4] Shyn *et al.*,[5] Register *et al.*,[7] Tanaka *et al.*,[27] and Gibson *et al.*[28] Between 10 and 30 eV, our calculated MTCS is in fair agreement with the values of Register *et al.*[7] and of Tanaka *et al.*[27] The small discontinuity near 19 eV is due to the changeover in $^2\Sigma_g$ symmetry from SEP results at lower energies to SE results. Some of the differences be-

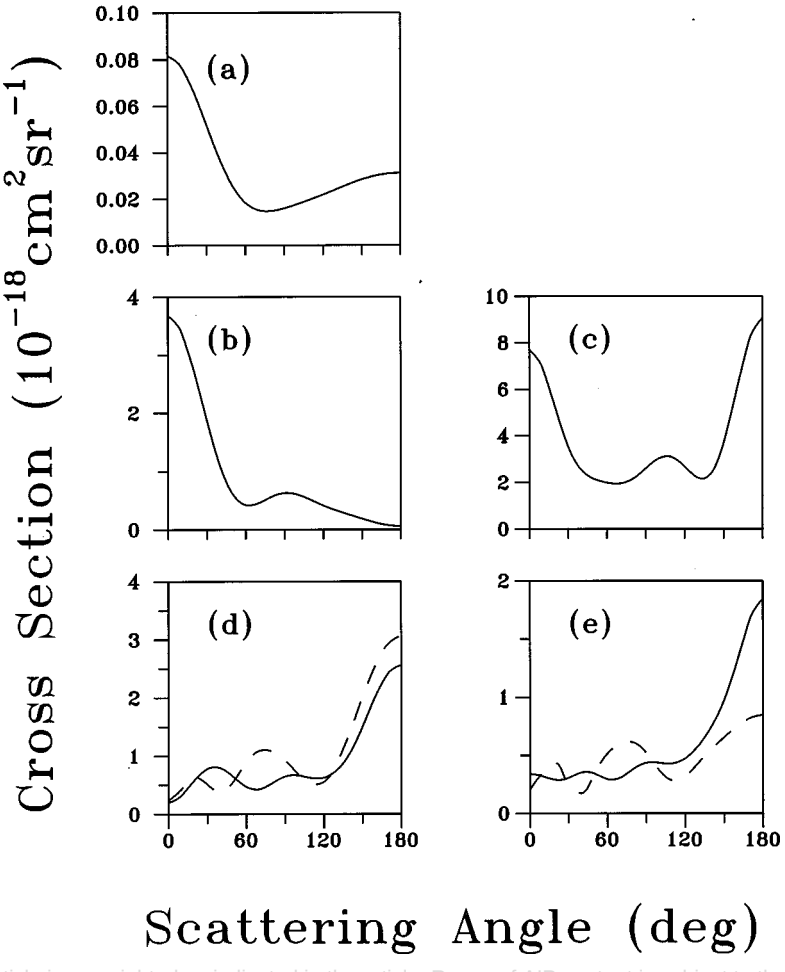

FIG. 10. Three-channel calculation of the $X\,^1\Sigma_g^+ \rightarrow {}^3\Sigma_u^+$ differential cross section at (a) 8.8 eV, (b) 13 eV, (c) 17.5 eV, (d) 28 eV, and (e) 40 eV. Solid line: present calculation. Dashed line: DW results of Ref. 50 at (d) 30 eV and (e) 40 eV.

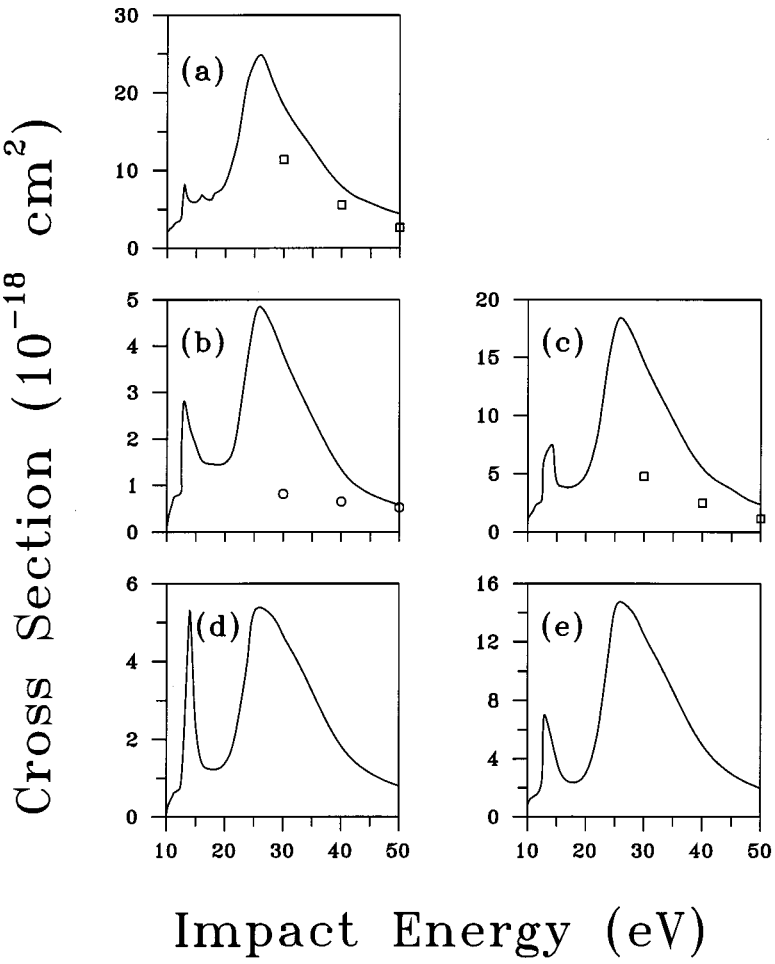

FIG. 11. Nine-channel calculation of the integral cross sections for (a) $X\,^1\Sigma_g^+ \rightarrow {}^3\Sigma_u^+$, (b) $X\,^1\Sigma_g^+ \rightarrow {}^1\Delta_u$, (c) $X\,^1\Sigma_g^+ \rightarrow {}^3\Delta_u$, (d) $X\,^1\Sigma_g^+ \rightarrow {}^1\Sigma_u^-$, and (e) $X\,^1\Sigma_g^+ \rightarrow {}^3\Sigma_u^-$. Circles represent DW results of Ref. 50 and squares represent Born results of Ref. 50.

tween our calculated values and those derived from experiment may arise from uncertainties in the extrapolation of the measured DCSs to 180°.

B. Three-channel calculation

We begin our discussion of the cross sections for electronic excitation of CO_2 with the results of a three-channel, two-state calculation which includes only the ground state ($X\,\Sigma_g^+$) and the lowest-lying excited state ($^3\Sigma_u^+$) as open channels. This three-channel calculation may provide a reasonable estimate of the cross section at impact energies for which the $^3\Sigma_u^+$ state is the only one accessible. Such threshold excitation cross sections are needed in many applications and can be difficult to measure.

Figure 9 shows the three-channel integral cross section for excitation of the $(1\pi_g \rightarrow 2\pi_u)\,^3\Sigma_u^+$ state of CO_2. The only other reported $^3\Sigma_u^+$ excitation cross sections are those of Lee and McKoy,[50] who used the distorted-wave (DW) approximation[90,91] to calculate the integral and differential cross sections at 30, 40, and 50 eV. Their results are also shown in Fig. 9. The integral cross section shows a pronounced peak near 17.5 eV collision energy, which is due to the $^2\Pi_g$ overall symmetry. Since the excited state symmetry is Σ_u^+, the peak is associated with a π_u scattering orbital in the exit channel, i.e., $^3\Sigma_u^+ \times {}^2\pi_u \rightarrow {}^2\Pi_g$. Partial wave analysis shows, moreover, that the dominant contribution is from $l=3$ in the exit channel. These features are consistent with an assignment of the 17.5 eV peak as a core-excited shape resonance having the configuration $[1\sigma_g^2 1\sigma_u^2 2\sigma_g^2 3\sigma_g^2 2\sigma_u^2 4\sigma_g^2 3\sigma_u^2 1\pi_u^4 1\pi_g^3 2\pi_u^2]$. As noted in Sec. III, the same configuration could also give rise to a $^2\Phi$ resonance not representable in our basis set. At higher energies, our results agree well with the DW results.

Figure 10 shows the calculated DCSs for excitation of the $^3\Sigma_u^+$ state at selected energies, along with the DW results[50] at 30 and 40 eV. At 8.8 eV, where $^3\Sigma_u^+$ is the only energetically accessible state, the DCS peaks in both the forward and the backward direction. Partial-wave analysis shows that both the *s* and *p* waves contribute strongly in this region. At 17.5 eV, near the maximum in the integral cross section, the DCS shows both forward and backward peaking, with minima at 70° and 130° and a maximum at 110°. The dominant contribution in this energy region is the *f*-wave from the $^2\Pi_g$ symmetry; however, contributions from other partial waves are also significant, and the observed pattern is not typical of *f*-wave scattering. At higher energies, both our results and the DW results show significant backward scattering, as is common for singlet→triplet excitations, although at lower scattering angles the two sets of results exhibit different angular patterns. Our partial-wave analysis indicates that the *p*, *d*, and *f* waves all contribute significantly in this energy region.

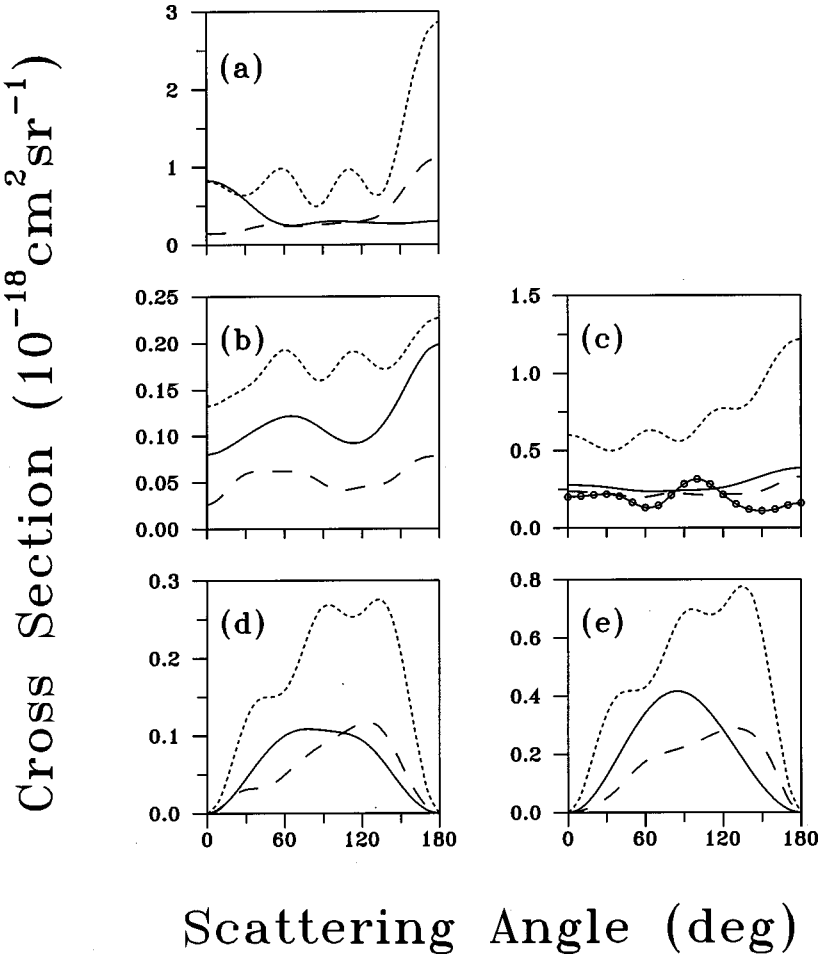

FIG. 12. Nine-channel calculations of the differential cross sections for electron energies of 13 eV (solid line), 28 eV (short dash), and 40 eV (long dash) for (a) $X\,^1\Sigma_g^+ \rightarrow {}^3\Sigma_u^+$, (b) $X\,^1\Sigma_g^+ \rightarrow {}^1\Delta_u$, (c) $X\,^1\Sigma_g^+ \rightarrow {}^3\Delta_u$, (d) $X\,^1\Sigma_g^+ \rightarrow {}^1\Sigma_u^-$, and (e) $X\,^1\Sigma_g^+ \rightarrow {}^3\Sigma_u^-$. Circles with solid line in (c) represent DW results of Ref. 50 at 40 eV.

C. Nine-channel calculation

In this section, we discuss the results of nine-channel, six-state calculations of cross sections for excitation of the $^3\Sigma_u^+$, $^3\Sigma_u^-$, $^1\Sigma_u^-$, $^1\Delta_u$, and $^3\Delta_u$ states that arise from the $1\pi_g \rightarrow 2\pi_u$ transition in CO_2. Coupling among these five states can be expected to be strong since they arise from the same elementary electronic transition.

Our calculated integral cross sections for electron-impact excitation to these states are shown in Figs. 11(a)–11(e). These cross sections are all dominated by two peaks, one at 12–13 eV and the other near 28 eV, both due to the $^2\Pi_g$ symmetry component. (Again, it should be noted that $^2\Phi$ and higher components are not present in the calculation.) In the three-channel calculation of the $^3\Sigma_u^+$ cross section discussed above, a single peak, also due to $^2\Pi_g$ symmetry, is seen at 17.5 eV. This qualitative change in the $^3\Sigma_u^+$ cross section clearly reflects strong coupling among the five electronically excited states included in the multichannel study. We also note that the magnitude of the cross section for the $^3\Sigma_u^+$ state is larger in the three-channel case than in the nine-channel case below 22 eV, while at higher energies, the nine-channel results are larger.

To gain insight into the composition of the two peaks in the integral cross sections of Fig. 11, we carried out partial-wave analyses of the associated scattering amplitudes. The first peak in the cross sections is associated with the *p*-wave ($l=1$) in the exit channel, while the second peak is associated with the *f*-wave ($l=3$).

The DW integral cross sections for the $^3\Sigma_u^+$ and the $^3\Delta_u$ states are also shown in Figs. 11(a) and 11(c), respectively. For both states, the DW results are smaller than those of the present calculation. For the $^1\Delta_u$ state, Lee and McKoy[50] reported two sets of cross sections: the DW results and the Born cross section. As seen in Fig. 11(b), our results are quite different from the Born cross section except at 50 eV. The DW integral cross section for this state is two orders of magnitude larger than our results and the Born results. As Lee and McKoy noted, such a large difference between the DW and Born results is unusual. Comparison with the present results provides further indication that the DW results for this state are too large.

The DCSs for excitation of the $^3\Sigma_u^+$ state are shown in Fig. 12(a). Comparing with the three-channel results in Fig. 10, we see that both sets of results exhibit somewhat similar structures, although their magnitudes differ. An examination of the three-channel and nine-channel DCSs at their respective resonance energy regions shows that the DCS at 17.5 eV in the three-channel calculation has a similar shape to the DCS at 28 eV in the nine-channel calculation. As mentioned earlier, both peaks are predominantly composed of the *f* wave ($l=3$) in the $^2\Pi_g$ symmetry. At 40 eV, both the three-channel and the nine-channel results, as well as the DW re-

sults, show the backward peaking often seen in singlet→triplet transitions. At scattering angles below 120°, both our three-channel and nine-channel DCSs are fairly flat, while the DW DCS has several features.

The DCSs for excitation of the $^1\Delta_u$, $^3\Delta_u$, $^1\Sigma_u^-$, and $^3\Sigma_u^-$ states are shown in Figs. 12(b)–12(e), respectively. The DW DCS for excitation of the $^3\Delta_u$ state at 40 eV is also shown in Fig. 12(c). For this state, the two sets of DCSs have similar magnitudes at low scattering angles, although their shapes differ. Our results exhibit stronger backward scattering than the DW results, with our DCS being about twice as large as the DW DCS at 180°. For the $^1\Delta_u$ state, the DW cross section at 40 eV is about two orders of magnitude larger than the present result. For the $^3\Sigma_u^-$ and $^1\Sigma_u^-$ states, the DCSs vanish at 0° and 180°, as required by the $\Sigma^+ \rightarrow \Sigma^-$ selection rule.[92] We also find that the ratio of the triplet to singlet cross sections is about three for both the Σ_u^- and Δ_u states. A similar ratio was observed for the transitions from the ground state to the $a\,^3A_2$ and $A\,^1A_2$ states of formaldehyde[57] as well as for the transitions from the ground state to the $I\,^1\Sigma^-$ and $e\,^3\Sigma^-$ states, and to the $D\,^1\Delta$ and $a\,^3\Delta$ states, of carbon monoxide.[58]

The large change in the $^3\Sigma_u^+$ cross section in going from the three-channel to the nine-channel coupling scheme indicates that the coupling among states arising from the $1\pi_g \rightarrow 2\pi_u$ transition is strong. A calculation that includes all open channels is impractical because the number of channels becomes large even at moderate energies. On the other hand, going beyond the nine-channel approximation would include electronic transitions not arising from the $1\pi_g \rightarrow 2\pi_u$ transition, whose coupling to the states arising from this transition may be weaker, resulting in smaller changes in the cross sections than were seen in going from the three- to the nine-channel approximation. Whether this is so can only be tested by further, more extensive calculations.

V. SUMMARY

We have employed the SMC variational method to calculate elastic cross sections for $e-CO_2$ collisions in the SEP approximation. Comparisons with measured values are generally good. Our description of polarization effects enables us to place the $^2\Pi_u$ resonance at the correct position without empirical adjustment. The dominant component of the resonance is found to be the *f* wave. We have also confirmed the existence of a virtual state near zero energy.

We have proposed a resolution to an apparent conflict between theory and experiment in the shape of the elastic DCS at low energies: The presence of the *s*-wave virtual state near zero energy implies isotropic DCSs, while the measured DCSs show strong forward scattering. We suggest that the forward scattering arises from significant population of vibrationally excited states of CO_2 that are on average bent and therefore have a dipole moment, resulting in enhanced forward scattering. Contributions from these vibrationally excited states are significant at typical experimental temperatures.

The SMC variational method was also used to calculate cross sections for electronically inelastic electron–CO_2 collisions leading to states arising from the $(1\pi_g \rightarrow 2\pi_u)$ transition. Results were reported for a two-state calculation $(X\,^1\Sigma_g^+, ^3\Sigma_u^+)$ and a six-state calculation $(X\,^1\Sigma_g^+, ^3\Sigma_u^+, ^1\Delta_u, ^3\Delta_u, ^3\Sigma_u^-, ^1\Sigma_u^-)$.

ACKNOWLEDGMENTS

This work was done on the Intel Touchstone Delta and the Intel Paragon systems operated by the Center for Advanced Computing Research (CACR) at Caltech, which is funded in part by the National Science Foundation, and on the CRAY T3D and the CRAY J916 of the Jet Propulsion Laboratory/California Institute of Technology Supercomputing Project. Financial support from the Air Force Office of Scientific Research (AFOSR) is gratefully acknowledged.

[1] M. Hayashi, in *Swarm Studies and Inelastic Electron–Molecule Collisions*, edited by L. C. Pitchford, B. V. McKoy, A. Chutjian, and S. Trajmar (Springer, New York, 1987), p. 167.
[2] E. Brüche, Ann. Phys. (Leipzig) **83**, 1065 (1927).
[3] C. Ramsauer, Ann. Phys. (Leipzig) **83**, 1129 (1927).
[4] J. J. Lowke, A. V. Phelps, and B. W. Irwin, J. Appl. Phys. **44**, 4664 (1973).
[5] T. W. Shyn, W. E. Sharp, and G. R. Carignan, Phys. Rev. A **17**, 1855 (1978).
[6] C. Szmytkowski and M. Zubek, Chem. Phys. Lett. **57**, 105 (1978).
[7] D. F. Register, H. Nishimura, and S. Trajmar, J. Phys. B **13**, 1651 (1980).
[8] J. Ferch, C. Masche, and W. Raith, J. Phys. B **14**, L97 (1981).
[9] K. R. Hoffman, M. S. Dababneh, Y.-F. Hsieh, W. E. Kauppila, V. Pol, J. H. Smart, and T. S. Stein, Phys. Rev. A **25**, 1393 (1982).
[10] Ch. K. Kwan, Y.-F. Hsieh, W. E. Kauppila, S. J. Smith, T. S. Stein, M. N. Uddin, and M. S. Dababneh, Phys. Rev. A **27**, 1328 (1983).
[11] O. Sueoka and S. Mori, J. Phys. Soc. Jpn. **53**, 2491 (1984).
[12] K.-H. Kochem, W. Sohn, N. Hebel, K. Jung, and H. Ehrhardt, J. Phys. B **18**, 4455 (1985).
[13] C. Szmytkowski, A. Zecca, G. Karwasz, S. Oss, K. Maciąg, B. Marinković, R. S. Brusa, and R. Grisenti, J. Phys. B **20**, 5817 (1987).
[14] I. Kanik, D. C. McCollum, and J. C. Nickel, J. Phys. B **22**, 1225 (1989).
[15] S. J. Buckman, M. T. Elford, and D. S. Newman, J. Phys. B **20**, 5175 (1987).
[16] M. A. Morrison, N. F. Lane, and L. A. Collins, Phys. Rev. A **15**, 2186 (1977).
[17] F. A. Gianturco, U. T. Lamanna, and S. Salvini, Int. J. Quantum Chem. **13**, 579 (1979).
[18] M. G. Lynch, D. Dill, J. Siegel, and J. L. Dehmer, J. Chem. Phys. **71**, 4249 (1979).
[19] D. Thirumalai, K. Onda, and D. G. Truhlar, J. Chem. Phys. **74**, 6792 (1981).
[20] L. A. Collins and B. I. Schneider, Phys. Rev. A **24**, 2387 (1981).
[21] R. R. Lucchese and V. McKoy, Phys. Rev. A **25**, 1963 (1982).
[22] L. A. Collins and M. A. Morrison, Phys. Rev. A **25**, 1764 (1982).
[23] F. A. Gianturco and T. Stoecklin, J. Phys. B **29**, 3933 (1996).
[24] F. A. Gianturco and R. R. Lucchese, J. Phys. B **29**, 3955 (1996).
[25] M. Takekawa and Y. Itikawa, J. Phys. B **29**, 4227 (1996).
[26] M. Kimura, O. Sueoka, A. Hamada, M. Takekawa, Y. Itikawa, H. Tanaka, and L. Boesten, J. Chem. Phys. **107**, 6616 (1997).
[27] T. Tanaka, T. Ishikawa, T. Masai, T. Sagara, L. Boesten, M. Takekawa, Y. Itikawa, and M. Kimura, Phys. Rev. A **57**, 1798 (1998).
[28] J. C. Gibson, M. A. Green, K. W. Trantham, S. J. Buckman, P. J. O. Teubner, and M. J. Brunger, J. Phys. B **32**, 213 (1999).
[29] M. J. W. Boness and G. J. Schulz, Phys. Rev. Lett. **21**, 1031 (1968).
[30] A. Andrick, D. Danner, and H. Ehrhardt, Phys. Lett. **29**, 346 (1969).
[31] A. Stamatovic and G. J. Schulz, Phys. Rev. **188**, 213 (1969).
[32] L. W. Larkin and J. B. Hasted, Chem. Phys. Lett. **5**, 325 (1970).
[33] M. J. W. Boness and G. J. Schulz, Phys. Rev. A **9**, 1969 (1974).
[34] I. Čadež, M. Tronc, and R. I. Hall, J. Phys. B **7**, L132 (1974).
[35] C. Szmytkowski and M. Zubek, J. Phys. B **10**, L31 (1977).
[36] I. Čadež, F. Gresteau, M. Tronc, and R. I. Hall, J. Phys. B **10**, 3821 (1977).
[37] M. Tronc, R. Azria, and R. Paineau, J. Phys. (France) **40**, L323 (1979).
[38] C. Szmytkowski, M. Zubek, and J. Drewko, J. Phys. B **11**, L371 (1978).

[39] D. Field, S. L. Lunt, G. Mrotzek, J. Randell, and J. P. Ziesel, J. Phys. B **24**, 3497 (1991).
[40] F. Currell and J. Comer, J. Phys. B **26**, 2463 (1993).
[41] W. M. Johnstone, P. Akther, and W. R. Newell, J. Phys. B **28**, 743 (1995).
[42] A. K. Kazansky and L. Y. Sergeeva, Z. Phys. D **37**, 305 (1996).
[43] Y. Itikawa, Phys. Rev. A **3**, 831 (1971).
[44] W. Domcke and L. S. Cederbaum, J. Phys. B **10**, L47 (1977).
[45] W. Domcke and L. S. Cederbaum, Phys. Rev. A **16**, 1465 (1977).
[46] M. A. Morrison and N. F. Lane, Chem. Phys. Lett. **66**, 527 (1979).
[47] D. Thirumalai, K. Onda, and D. G. Truhlar, J. Phys. B **13**, L619 (1980).
[48] D. Thirumalai and D. G. Truhlar, J. Chem. Phys. **75**, 5207 (1981).
[49] E. S. Chang, J. Phys. B **17**, 3341 (1984).
[50] M.-T. Lee and V. McKoy, J. Phys. B **16**, 657 (1983).
[51] K. Takatsuka and V. McKoy, Phys. Rev. A **24**, 2473 (1981).
[52] K. Takatsuka and V. McKoy, Phys. Rev. A **30**, 1734 (1984).
[53] C. Winstead and V. McKoy, in *Modern Electronic Structure Theory*, edited by D. R. Yarkony (World Scientific, Singapore, 1995), p. 1375.
[54] C. Winstead, Q. Sun, and V. McKoy, J. Chem. Phys. **98**, 1105 (1993).
[55] C. Winstead, Q. Sun, V. McKoy, J. L. S. Lino, and M. A. P. Lima, Z. Phys. D **24**, 141 (1992).
[56] H. P. Pritchard, V. McKoy, and M. A. P. Lima, Phys. Rev. A **41**, 546 (1990).
[57] Q. Sun, C. Winstead, V. McKoy, J. S. E. Germano, and M. A. P. Lima, Phys. Rev. A **46**, 2462 (1992).
[58] Q. Sun, C. Winstead, and V. McKoy, Phys. Rev. A **46**, 6987 (1992).
[59] C. Winstead, Q. Sun, V. McKoy, J. L. S. Lino, and M. A. P. Lima, J. Chem. Phys. **98**, 2132 (1993).
[60] C. Winstead, H. P. Pritchard, and V. McKoy, J. Chem. Phys. **101**, 338 (1994).
[61] D. Danner, Diplomarbeit, Universität Freiburg, 1970.
[62] D. Andrick and F. H. Read, J. Phys. B **4**, 389 (1971).
[63] M. A. Morrison, Phys. Rev. A **25**, 1445 (1982).
[64] B. L. Whitten and N. F. Lane, Phys. Rev. A **26**, 3170 (1982).
[65] H. Estrada and W. Domcke, J. Phys. B **18**, 4469 (1985).
[66] L. A. Morgan, Phys. Rev. Lett. **80**, 1873 (1998).
[67] C. Winstead and V. McKoy, Adv. At., Mol., Opt. Phys. **36**, 183 (1996).
[68] C. Winstead and V. McKoy, Phys. Rev. A **57**, 3589 (1998).
[69] B. I. Schneider and L. A. Collins, Phys. Rev. A **30**, 95 (1984).
[70] T. H. Dunning, Jr., J. Chem. Phys. **53**, 2823 (1970).
[71] A. D. McLean and M. Yoshimine, IBM J. Res. Dev. **12**, 206 (1967).
[72] W. J. Hunt and W. A. Goddard III, Chem. Phys. Lett. **3**, 414 (1969).
[73] W. J. Hunt, Ph.D. thesis, California Institute of Technology, Pasadena, CA, 1972.
[74] N. W. Winter, C. F. Bender, and W. A. Goddard III, Chem. Phys. Lett. **20**, 489 (1973).
[75] W. B. England and W. C. Ermler, J. Chem. Phys. **70**, 1711 (1979).
[76] J. W. Rabalais, J. M. McDonald, V. Scherr, and S. P. McGlynn, Chem. Rev. **71**, 73 (1971).
[77] R. I. Hall, A. Chutjian, and S. Trajmar, J. Phys. B **6**, L264 (1973).
[78] D. Dill and J. L. Dehmer, J. Chem. Phys. **61**, 692 (1974).
[79] H.-D. Meyer, S. Pal, and U. V. Riss, Phys. Rev. A **46**, 186 (1992).
[80] K. B. Ghose, S. Pal, and H.-D. Meyer, J. Chem. Phys. **99**, 945 (1993).
[81] Y. Singh, J. Phys. B **3**, 1222 (1970).
[82] I. I. Fabrikant, J. Phys. B **17**, 4223 (1984).
[83] E. Gerjuoy and S. Stein, Phys. Rev. **97**, 1671 (1955).
[84] L. Wijnberg, J. Chem. Phys. **44**, 3864 (1966).
[85] M. Hayashi and Y. Nakamura (private communication).
[86] J. Ferch, C. Masche, W. Raith, and L. Wiemann, Phys. Rev. A **40**, 5407 (1989).
[87] W. M. Johnstone, N. J. Mason, and W. R. Newell, J. Phys. B **26**, L147 (1993).
[88] L. A. Gribov and W. J. Orville-Thomas, *Theory and Methods of Calculation of Molecular Spectra* (Wiley, New York, 1988), p. 318.
[89] A. Herzenberg, J. Phys. B **1**, 548 (1968).
[90] A. W. Fliflet and V. McKoy, Phys. Rev. A **21**, 1863 (1980).
[91] M. T. Lee, R. R. Lucchese, and V. McKoy, Phys. Rev. A **26**, 3240 (1982).
[92] D. C. Cartwright, S. Trajmar, W. Williams, and D. L. Huestis, Phys. Rev. Lett. **27**, 704 (1971).